

RESEARCH

Open Access



# Orbital mesenchymal chondrosarcoma and its specific fusion gene *HEY1-NCOA2*

Jia-Qi Lin<sup>1</sup>, Xun Liu<sup>1</sup>, Jin-Zhi Zhao<sup>1</sup>, Qing Wang<sup>1</sup>, Li-Min Zhu<sup>1\*</sup> and Ting-Ting Lin<sup>1\*</sup>

## Abstract

**Background** Mesenchymal chondrosarcoma (MC) is an uncommon type of malignant soft tissue tumor. The skeleton is the most common site of MC. Extrasosseous sarcoma is rare, especially that of the orbit. Fusion gene HEY1–NCOA2 has diagnostic significance for MC, but there is a lack of research on its related pathways. To analyze the characteristics of orbital mesenchymal chondrosarcoma (MC), and search for HEY1-NCOA2-related pathways in orbital MCs, four cases of orbital MC were included in the study.

**Methods** From January 2018 to December 2022, four MC patients hospitalized at Tianjin Medical University Eye Hospital were collected for a retrospective series of case studies. HEY1-NCOA2 of the assay specimens was detected by fluorescence in situ hybridization, and immunohistochemical staining was performed for representative proteins of the relevant pathways. For figure modification and statistical analysis, GraphPad Prism 8.0 (La Jolla, CA, USA) was utilized.

**Results** Four orbital MC were reported. Among the 4 ligible MC specimens, two were HEY1-NCOA2-positive and two were HEY1-NCOA2-negative. Immunohistochemistry showed stronger expression of COL2A1, APC, CD99, and Bcl2 in HEY1-NCOA2-positive samples than in HEY1-NCOA2-negative MCs.

**Conclusion** We summarized the clinical features, treatments, and prognosis of orbital MC, including our cases and the literature. The expression of COL2A1 and Bcl2 is elevated in HEY1-NCOA2-positive tissues, and they promote tumor cell growth by regulating cell proliferation, apoptosis, epithelial–mesenchymal transition, and drug resistance. For HEY1-NCOA2-positive patients, given the high expression of CD99, drugs targeting the MAPK pathway may be an effective treatment.

**Keywords** Mesenchymal chondrosarcoma, HEY1-NCOA2, Fluorescence in situ hybridization, Small undifferentiated cells, Chondrocytes, Orbital tumor

\*Correspondence:

Li-Min Zhu  
zlmjojo@163.com  
Ting-Ting Lin  
litt6123@126.com

<sup>1</sup>Tianjin Key Laboratory of Retinal Functions and Diseases, Tianjin Branch of National Clinical Research Center for Ocular Disease, Eye Institute and School of Optometry, Tianjin Medical University Eye Hospital, Tianjin 300384, China



© The Author(s) 2025. **Open Access** This article is licensed under a Creative Commons Attribution-NonCommercial-NoDerivatives 4.0 International License, which permits any non-commercial use, sharing, distribution and reproduction in any medium or format, as long as you give appropriate credit to the original author(s) and the source, provide a link to the Creative Commons licence, and indicate if you modified the licensed material. You do not have permission under this licence to share adapted material derived from this article or parts of it. The images or other third party material in this article are included in the article's Creative Commons licence, unless indicated otherwise in a credit line to the material. If material is not included in the article's Creative Commons licence and your intended use is not permitted by statutory regulation or exceeds the permitted use, you will need to obtain permission directly from the copyright holder. To view a copy of this licence, visit <http://creativecommons.org/licenses/by-nc-nd/4.0/>.

## Introduction

Mesenchymal chondrosarcoma (MC), a rare malignant neoplasm characterized by a bimorphic pattern that is composed of poorly differentiated small round cells and islands of well-differentiated hyaline cartilage, can appear in various parts of the body. The skeleton is the most common site of MC, but it also can arise from extraskel-etal sites. It has been reported since skeletal MC was discovered by Lichtenstein et al. [1] in 1959. Reech et al. [2] reported a case of a 27-year-old white female with MC of the orbit in 1966, which is the first example of orbital MC to be documented. In 2012, Robert Nakayama et al. discovered a specific fusion gene *HEY1-NCOA2* in MCs, and the diagnostic significance of this fusion gene for MC was proposed [3]. Thereafter, the presence of the fusion gene *HEY1-NCOA2* was verified in bone and extraosseous soft tissues [4]. A recent study [5], based on iPSC-derived mesenchymal stem cells (iPSC-MSCs), explored the role of *HEY1-NCOA2* in pathway transduction and found that *HEY1-NCOA2* may have an activating effect on target genes that are repressed by wild-type *HEY1*.

This article describes four cases of MC occurring in orbital soft tissue and summarizes and analyzes the clinical aspects of MC. Furthermore, we used rolling circle amplification fluorescence in situ hybridization (RCA-FISH) to detect the fusion gene *HEY1-NCOA2* in the specimens obtained during surgery, and we explored the pathways related to MC and the specific fusion gene *HEY1-NCOA2* via immunohistochemistry.

## Materials and methods

### Case selection

This study was approved by Medical Ethics Committee of Tianjin Medical University Eye Hospital (2022KY [L]-59). From January 2018 to December 2022, the clinical and follow-up data of four MC patients hospitalized at Tianjin Medical University Eye Hospital were collected for a retrospective series of case studies. Excision of the mass was performed for all patients. Hematoxylin–eosin (HE) and immunohistochemical staining of the specimens were performed after surgery. The follow-up period ends on December 31, 2022.

### Potentially activated pathways in MC

Paraffin-embedded tissues were collected from the Tianjin Medical University Eye Hospital. The histological diagnosis was MC.

### RCA-FISH

According to the method described by Larsson et al. [6], a large number of linearly cyclized Padlock probes are amplified. The linear cyclization probe of *HEY1* binds to the fluorescent probe Alex488 (Thermo) and is labeled in green; the linear cyclization probe of *NCOA2* binds to

the fluorescent probe Cy3 (Thermo) and is labeled in red. A total of 100 interphase nuclei from each tumor specimen were analyzed. The complete signal overlap of *HEY1* and *NCOA2* reached more than 20%, and we considered the specimen positive for the fusion gene because *HEY1* and *NCOA2* were on the same chromosome, separated by only 10 Mb in length [7, 8].

### Immunohistochemistry

Representative proteins of each pathway expression in MC tissues were detected by immunohistochemistry. We stained Notch homolog 1 (Notch1, 1:200, Affinity), Collagen Type II (COL2A1, 1:1000, Proteintech), SRY-Box Transcription Factor 9 (SOX9, 1:100, Affinity), Wingless/Integrated 3a (WNT3A, 1:100, Affinity),  $\beta$ -catenin (ZSGB-BIO), adenomatous polyposis coli (APC, ZSGB-BIO), protein kinase C (PKC- $\alpha$ , 1:100, Affinity), CD99 (ZSGB-BIO), B-cell lymphoma-2 (Bcl2, ZSGB-BIO), transforming growth factor- $\beta$  (TGF- $\beta$  1, 1:100, Affinity), plasminogen activator inhibitor-1 (PAI-1, 1:200, Proteintech), phospho-Smad2 (p-Smad2, 1:100, Affinity), phospho-Smad1 (p-Smad1, 1:100, Affinity), platelet-derived growth factor receptor  $\alpha$  (PDGFR $\alpha$ , ZSGB-BIO), protein kinase B (AKT, 1:200, Proteintech), phospho-AKT (p-AKT, 1:200, Proteintech), phospho-mammalian target of rapamycin (p-mTOR, rabbit, 1:100, Affinity), glutamine synthetase (GS, ZSGB-BIO), phosphoinositide 3-kinase (PI3K, 1:500, Proteintech), and hairy and enhancer of split 1 (HES1, 1:100, Affinity). A 4  $\mu$ m-thick section was cut from the three different paraffin-embedded tissues of each specimen. Paraffin sections were obtained for routine dewaxing and rehydration. DAB reagent was used to color the tissues, and hematoxylin was used to re-stain the tissues. The immunohistochemical results were scored.

### Statistical analyses

For figure modification and statistical analysis, GraphPad Prism 8.0 (La Jolla, CA, USA) was utilized.  $P < 0.05$  was regarded as statistically significant.

## Results

### Clinical presentation of four patients

Details of the four cases are shown in the figures. Three of our cases were middle-aged women (40–47 years old) and one case was an 11-year-old boy. The tumors of the four cases were all located in the upper orbit. The three on the temporal side, whereas the mass of case 4 was located on the nasal side.

### Case 1

Hyperdensity was observed in CT examinations. The optic nerve and tumor were poorly delineated, and the tumor compressed the optic nerve and orbital wall,

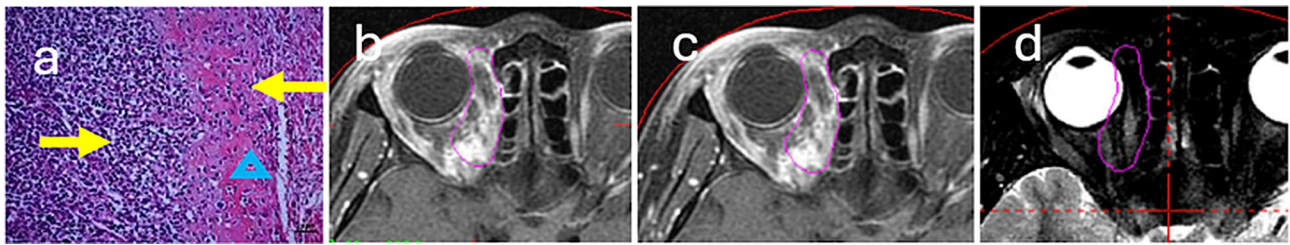


**Fig. 1** Case 1. (a) Histopathology of recurrent specimen (H&E staining, original magnification  $\times 20$ ), yellow  $\rightarrow$ , undifferentiated mesenchymal round cells; blue  $\rightarrow$ , areas of immature cartilage;  $\Delta$ , antler-like vascular gaps; (b and c) MRI images at 1 month and 1.5 years after recurrent surgery show that the soft tissue of the right orbit is nonhomogeneous slightly hyperintense in the axial scan of the orbit on the T1-weighted image of the right orbit, with no significant change in 1.5 years; (d) MRI at 1.5 years after recurrent surgery shows that the internal rectus muscle is widened and isointense in the axial scan of the orbit on the T2-weighted image of the right orbit

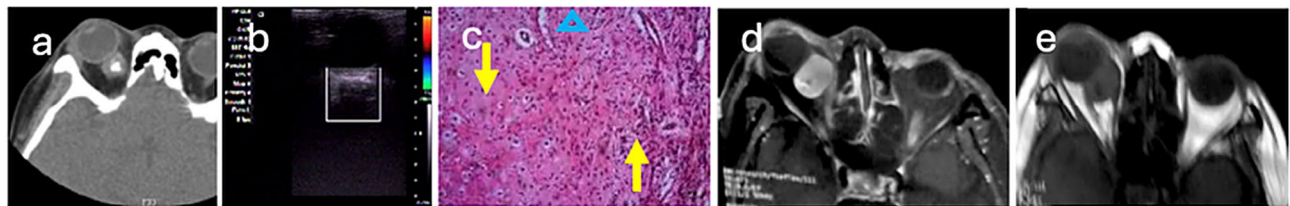


**Fig. 2** Case 2. (a) CT image before the first surgery shows a circular-like lesion with a hyperdense supraorbital area in the axial scan of the orbit; (b) CDU before surgery shows an irregular hypoechoic to isoechoic mass with well-defined border behind the eyeball, in which there is acoustic attenuation behind the hyperechoic mass, the optic nerve is compressed to the inferior temporal area, the wall of the eyeball is sunken under pressure, and there is no blood flow in the mass; (c) Histopathology of the specimen of first surgery ( $\times 20$ ), yellow  $\rightarrow$ , undifferentiated mesenchymal round cells; blue  $\rightarrow$ , areas of immature cartilage;  $\Delta$ , antler-like vascular gaps; (d and e) MRI of 2 years after first surgery shows an irregular hyperintense lesion of 3 cm  $\times$  3 cm in the muscle cone behind the right eyeball, compressing the optic nerve to displace to the nasal side in the axial scan of the orbit on T1-weighted image. The lesion is hyperintense compressing adjacent extraocular muscle to displace on T2-weighted image

causing bone erosion. Resection of the tumor was performed after the first onset, and no postoperative radiotherapy or chemotherapy was performed. The tumor recurred 2 years later. After recurrence, the lesion adhered to the surrounding tissues (levator palpebrae muscle and superior oblique muscle), and enlarged resection of the mass was performed. Postoperatively, the patient underwent adjuvant  $\gamma$ -knife treatment, and the follow-up showed gradual reduction of the tumor, with regular postoperative MRI. She was followed up for 4 years after surgery without recurrence (Fig. 1).

### Case 2

The patient underwent radical orbital excision. Intraoperatively, the mass was round and white, with an uneven surface, hard texture, and no obvious adhesions with the surrounding tissues. After 1 year and 9 months postoperatively, a local recurrence of the tumor was found, and he underwent another orbital excision in another hospital (Fig. 2).

### Case 3

MRI was performed in both cases 3, the mass was in the superior orbit behind the right eyeball, with isointense on the T1-weighted image (T1WI) and T2-weighted image (T2WI). The patient underwent an orbital mass excision. Intraoperatively, the mass was dark red cauliflower-like,

with a smooth surface, a tough false envelope, and obvious adhesions to the surrounding tissues. He had radiotherapy and chemotherapy after surgery and was followed up for 1 year and 9 months without recurrence (Fig. 3).

### Case 4

The tumor adhered to the surrounding tissue when it first appeared, and no adjuvant treatment was performed after surgical resection. After 2.5 years, the tumor recurred and was resected again. Intraoperatively, the tumor was found to be closely attached to the external rectus muscle and invaded the orbital apex. It was purplish-red lobulated mass with a false envelope. Several rounded ossified tissues were seen within it, adhering to the surrounding tissue. The patient underwent 28 sessions of systemic radiotherapy after the second surgery following up with CT and MRI. MRI at 3 months after the second surgery showed that the left lateral orbital soft tissue was slightly thickened with isointensity on T1WI and slight hyperintensity on T2WI after fat suppression. The MRI examinations at 6, 13, and 18 months postoperatively showed no significant changes compared with 3 months (Fig. 4, Supplementary material 1–1).

We collected a total of five specimens (three cases of first occurrence and two cases of recurrence). In the recurrent specimen of case 4, several white, hard nodules

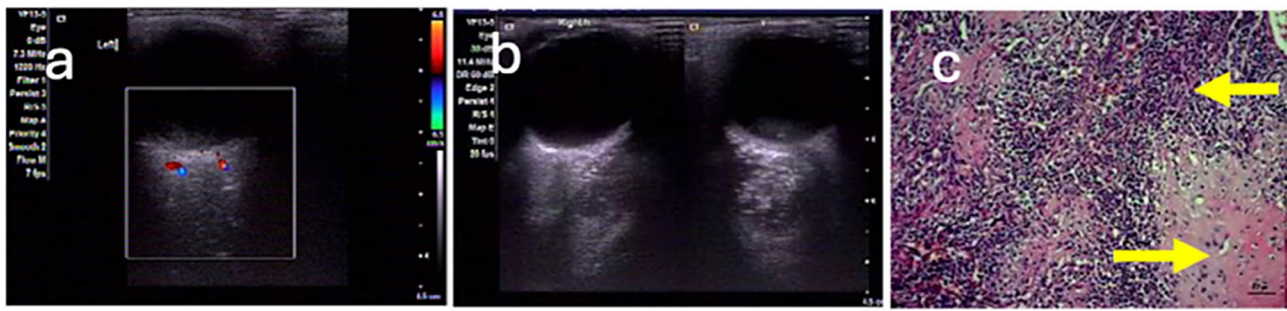


**Fig. 3** Case 3. (a and b) CDFI before surgery shows an irregular hypoechoic mass with well-defined border behind the eyeball, with patchy isoechoic to hyperechoic nodules. The optic nerve is compressed to the inferior nasal area, and there is no blood flow in the mass; (c) Histopathology of the specimen ( $\times 20$ ), yellow  $\rightarrow$ , undifferentiated mesenchymal round cells; blue  $\rightarrow$ , areas of immature cartilage

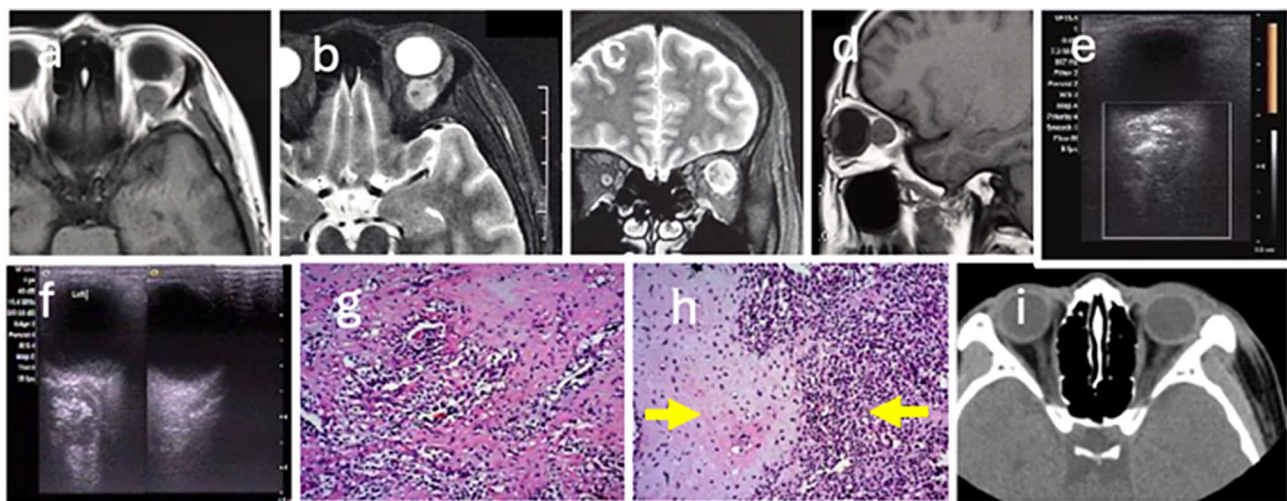


**Fig. 4** Case 4. (a and b) MRI before first surgery shows a circular-like isointense lesion with a size of 1.4 cm  $\times$  1.5 cm located in the superior temporal area of the muscle cone behind the eyeball, compressing the optic nerve in the axial scan of the orbit on T1- and T2-weighted images. (c) MRI before first surgery shows nonhomogeneous enhancement of the lesion in the axial and coronal scan of the T2-weighted image. (d) MRI before first surgery shows a circular-like lesion located in the superior temporal area of the muscle cone behind the eyeball in the sagittal scan of the T1-weighted image. (e and f) CDFI before first and second surgeries show the irregular isoechoic to hyperechoic mass with well-defined border behind the eyeball, and the optic nerve is compressed to displace to the nasal temporal area at the time of the relapse. (g and h) Histopathology show a large percentage of undifferentiated mesenchymal cells, which were elliptical or short shuttle in first specimen, and stratified distribution in the recurrent specimen ( $\times 20$ ), yellow  $\rightarrow$ , undifferentiated mesenchymal round cells; yellow  $\rightarrow$ , areas of immature cartilage; (i) CT image of 8 months after the second surgery, axial scan of the orbit on soft tissue window, and slight thickening of soft tissue in the temporal aspect of the left orbit

were observed. The maximum diameter of the five masses was 1.5–3.8 cm. The specimen contained small undifferentiated cells, chondrocytes, and ossification, or small undifferentiated cells as the main component. Heman-giopericytomas were observed in small undifferentiated cell regions in the five specimens. Necrosis was rare (Figs. 1a, 2c and 3c, and 4g–h).

**Fusion gene HEY1-NCOA2 and potentially activated pathways in MC**

**RCA-FISH detection of HEY1-NCOA2 fusion in MCs**

Complete signal overlap was  $<10\%$  in case 4 of recurrence, 15.79% in case 1 of recurrence, 62.03% in case 3, and 62.07% in case 4 at the time of first onset. The specimen from case 2 was excluded because of the presence

of ossified components and high protein loss after tissue decalcification treatment (Fig. 5).

**Immunohistochemistry**

We divided the specimens into two groups using 20% HEY1-NCOA2-positive rate as the limit [7, 8]: the HEY1-NCOA2-positive group included specimens from cases 3 and 4 at the time of first onset, and the negative group included specimens from cases 1 and 4 at the time of recurrence (Figs. 6 and 7).

**Discussion**

**Orbital MC**

About one-fifth to one-third of MCs occur in extraosseous soft tissue. Cerebrospinal membrane and lower

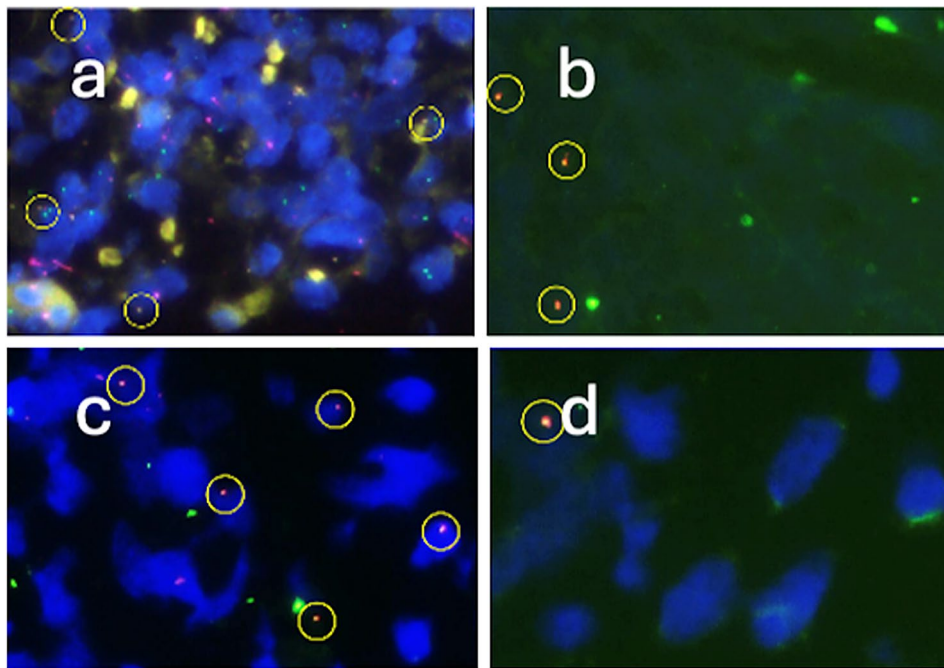


**Fig. 5** HEY1-NCOA2 RCA-FISH analysis: yellow circles, the positive signals appear as a single fused dot. (a) Recurrent specimen of case 1 shows complete signal overlap of 15.79%; (b) Specimen of case 2 the complete signal overlap is 62.03%; (c and d) Specimen of case 4 in first surgery and recurrent specimen show complete signal overlap 62.07% and < 10%

extremities are the most common locations for MC, followed by the orbit, parietal iliac soft tissue, and paravertebral soft tissue. Orbital MCs usually originate from stromal cells in the orbit. Combined with literature search from 2002 Jan1 to 2022 Dec31, 36 cases of MC involving the orbit were found. Four cases were current, and 32 cases [3, 9–34] were from the literature (Supplementary material 2–1). The epidemiological results are shown in figure (Fig. 8a–b and Supplementary material 2–2).

All 36 patients had monocular disease. The first episode duration was  $11.61 \pm 24.67$  months (Supplementary material 2–3). Notably, one female infant among our statistical cases is the only one reported so far with congenital onset of orbital MC. Proptosis, decreased vision, and papilledema were the most common symptoms or signs (Fig. 8c and Supplementary material 2–4).

On imaging, MC appears close to soft tissue. (Tables 1 and 2 and Supplementary materials 2–5, 6, 7, 8) We observed mass or stripe hypointensity mixed on both T1WI and T2WI, which corresponded to the hyperdense area on the CT scan. This result corresponded to the ossification composition of the specimen. Several stripe hyperintense areas are enhanced in T2WI, corresponding to hemangiopericytoma. Parts other than these areas exhibited obvious enhancement. In the orbit, the mass is most often located in the superior medial and superior lateral quadrants. On the basis of the patient's clinical presentation and imaging, the mass was most likely to be

misdiagnosed as cavernous hemangioma before surgery (Supplementary material 2–9).

Surgical resection is the main treatment of MC, including excision and exenteration. And radiotherapy and chemotherapy are important adjuvant treatments. Immunohistochemistry results in the current case 3 showed a Ki67 of 30%, which was higher compared with the other cases, but the patient had postoperative radiation and chemotherapy and no recurrence to date. The ratio of well-defined to ill-defined demarcation of the mass from the surrounding tissue was about 1:2 in first and recurrent surgery (Fig. 8d). The mass was mostly adherent to the optic nerve, extraocular muscles, and orbital wall. Bagheri et al. [19] reported a case in which the mass adhered to the dura mater at the time of recurrence (Supplementary material 2–10).

A total of 35 patients were subjected to pathological examination. (Supplementary material 2–11). Six cases had a smooth surface or complete pseudo-envelope, and six cases had a rough surface or incomplete envelope. Most of the masses were solid gray white in sections with hard nodules that may be accompanied with hemorrhage and necrosis (Supplementary material 2–12).

Microscopically, MC shows a typical biphasic pattern consisting of undifferentiated small round or oval cells mixed with hyaline chondrocytes (Supplementary material 2–13). There is a transition zone or a clear demarcation between the two components. Osteoclastic components are likely to be present.

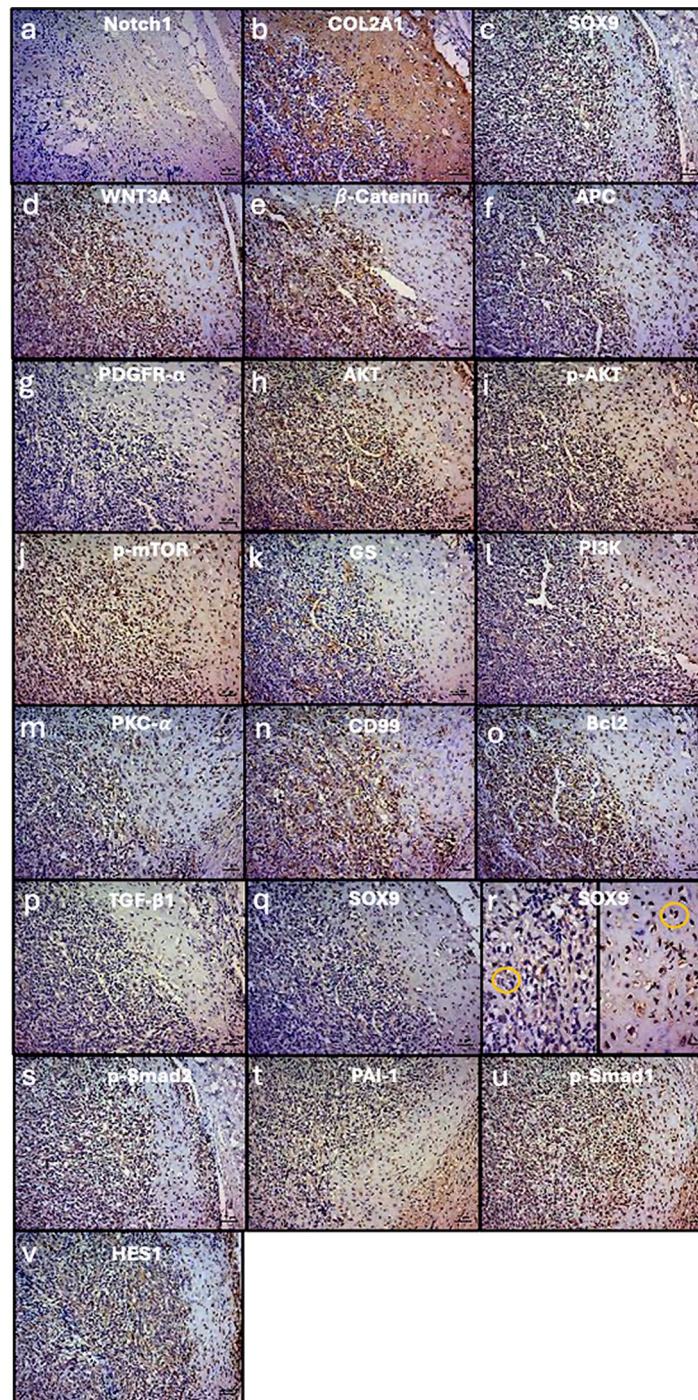


**Fig. 6** Immunohistochemistry, expression of pathway-related proteins in undifferentiated mesenchymal cells (left) and cartilage (right) regions. **Notch signaling** (a, × 20) Negative for Notch1; (b, × 20) Positive for COL2A1 in the extracellular region, and high percentage of positive cells in the cartilage region; (c, × 20) Nuclear positive for SOX9. **Wnt/β-Catenin** (d, × 20) Positive for WNT3A in the extracellular region; (e, × 20) Nuclear and cytoplasmic positive for β-Catenin, and high percentage of positive cells in the undifferentiated mesenchymal round cell region; (f, × 20) Nuclear and membrane positive for APC, and high percentage of positive cells in the undifferentiated mesenchymal round cell region. **PI3K/AKT/mTOR** (g, × 20) Negative for PDGFR $\alpha$ ; (h, × 20) Nuclear, membrane, and cytoplasmic positive for AKT; (i, × 20) Nuclear, membrane, and cytoplasmic positive for p-AKT, and high percentage of positive cells in the cartilage region; (j, × 20) Nuclear and cytoplasmic positive for p-mTOR; (k, × 20) Positive for GS, and cartilage cells are negative for GS; (l, × 20) Membrane and cytoplasmic positive for PI3K; (m, × 20) Nuclear, membrane, and cytoplasmic positive for PKC- $\alpha$ ; (n, × 20) Membrane positive for CD99, and high percentage of positive cells in the undifferentiated mesenchymal round cell region; (o, × 20) Nuclear positive for Bcl2, and high percentage of positive cells in the undifferentiated mesenchymal round cell region. **TGF-β/BMP** (p, × 20) Negative for TGF- $\beta$ 1; (q, × 20) Nuclear positive for SOX9; (r, × 40) Clear demonstration of positive expression of SOX9; (s, × 20) Nuclear and cytoplasmic positive for p-Smad2; (t, × 20) Positive for PAI-1 in the extracellular region; (u, × 20) Nuclear and cytoplasmic positive for p-Smad1. **HES1** (v × 20) Nuclear positive for HES1

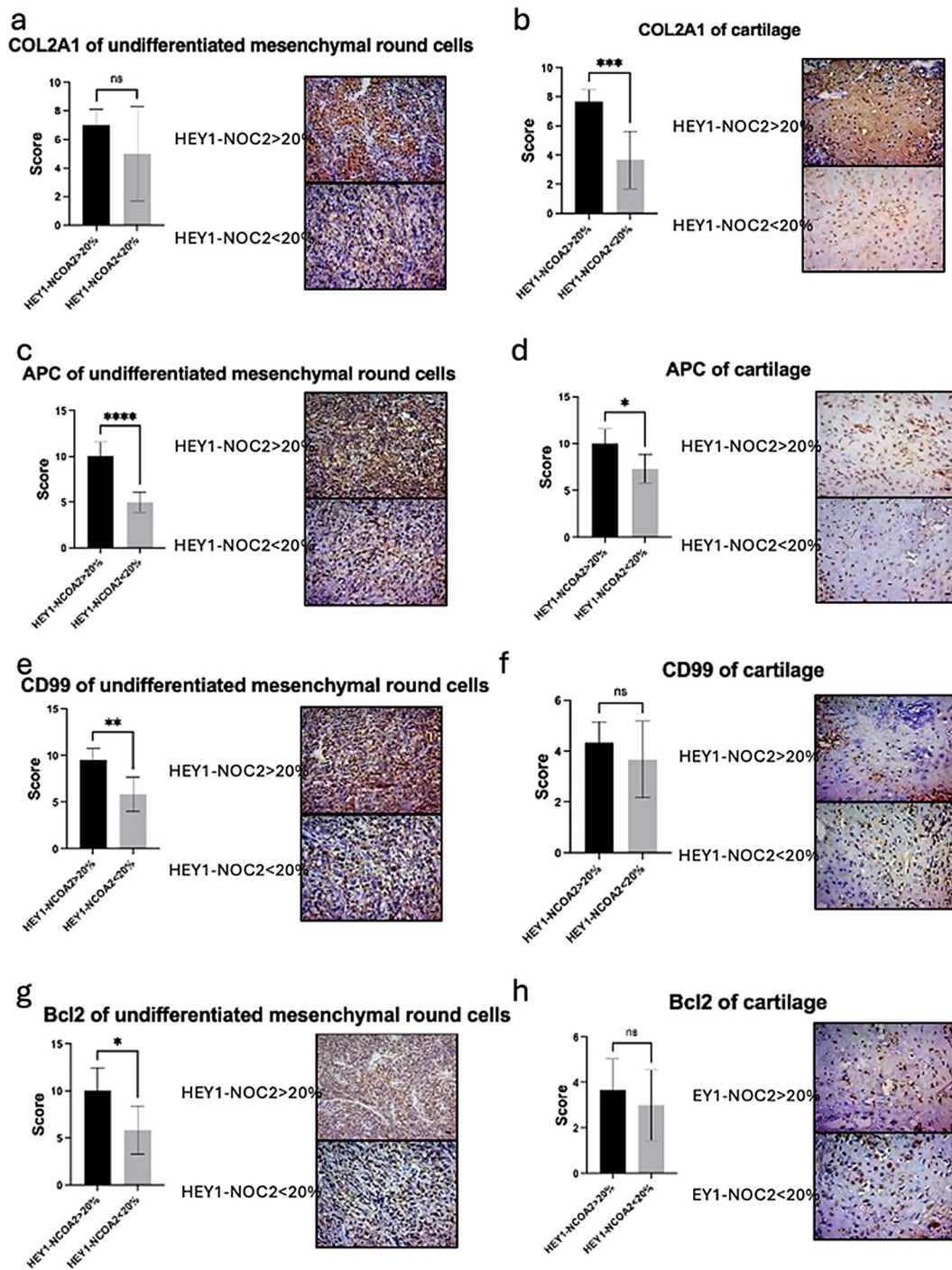


**Fig. 7** Effect of HEY1-NCOA2 positivity on proteins expression in MC. **COL2A1** (a) in the undifferentiated mesenchymal round cell region (ns,  $P > 0.05$ ) and (b) in the cartilage region ( $***P \leq 0.001$ ); **APC**: (c) in the undifferentiated mesenchymal round cell region ( $****P < 0.0001$ ) and (d) in the cartilage region ( $*P < 0.05$ ); **CD99**: (e) in the undifferentiated mesenchymal round cell region ( $**P < 0.01$ ) and (f) in the cartilage region (ns,  $P > 0.05$ ); **Bcl2**: (g) in the undifferentiated mesenchymal round cell region ( $*P < 0.05$ ) and (h) in the cartilage region (ns,  $P > 0.05$ )

Small undifferentiated cells with blue HE staining exhibited large darkly stained nucleus, which was heterotopic and mitotic. Cells were round, ovoid, or spindle in shape, and the cytoplasm is basophilic. The cells were uniform in size, and part of them surrounded the vessels

to mimic a hemangiopericytoma; occasionally [17, 29, 31], antler-like vascular gaps were observed. The cartilage component was composed of differentiated mature or immature chondrocytes. Chondrocytes were heterogeneous and eosinophilic, with dark-stained nuclei. They

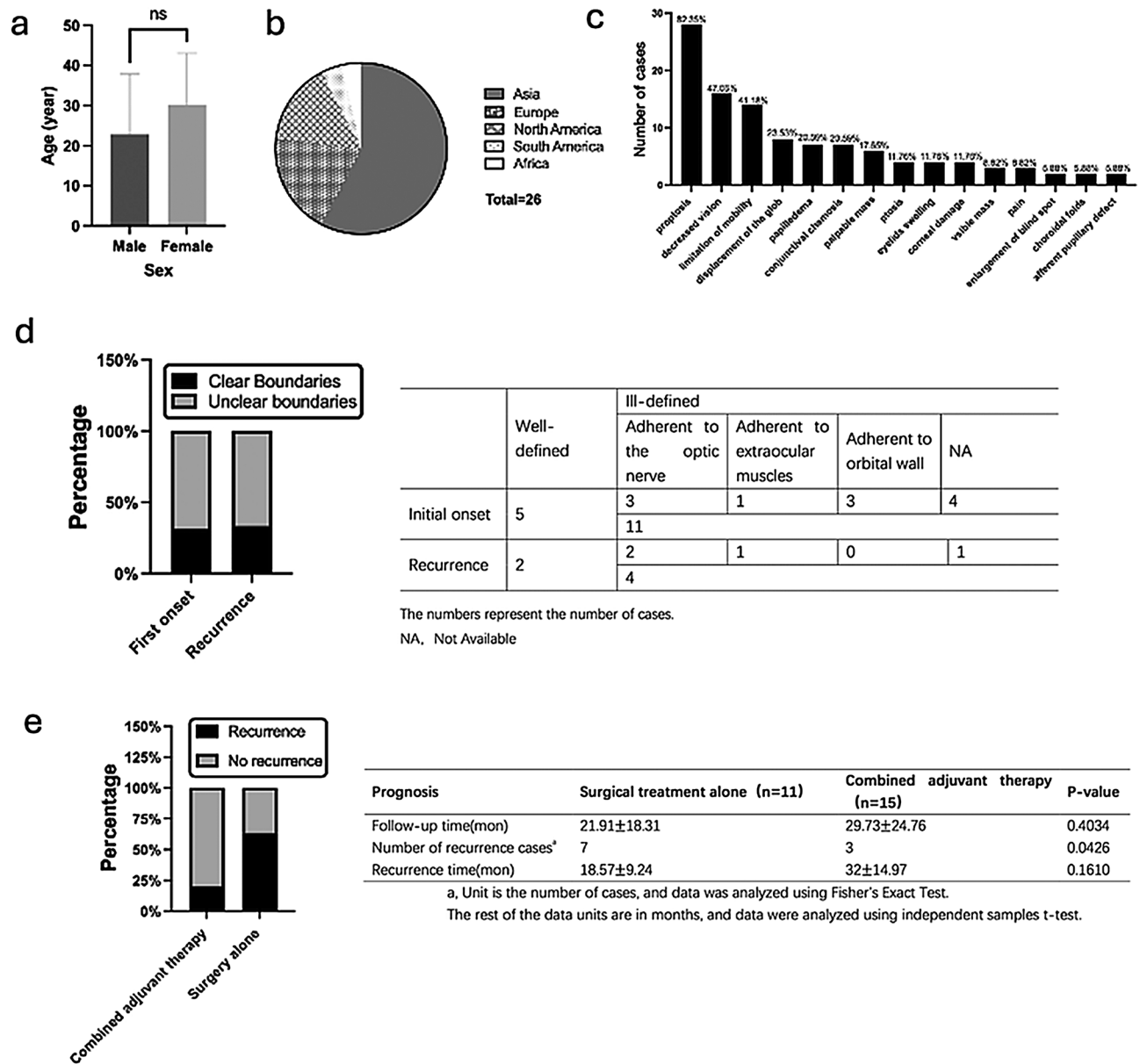


**Fig. 8** Clinical features of MC. **(a)** Age profile of male and female patients; **(b)** regional distribution of patients with orbital MC; **(c)** symptoms and signs of orbital MC; **(d)** borders of orbital MC with surrounding tissues at first onset and recurrence; and **(e)** prognosis of patients who underwent surgery alone and adjuvant therapy after surgery

could form cartilage islands with irregular foci of punctate calcification as the ossification component. A transition zone was noted between small undifferentiated cells and chondrocytes, or a clear demarcation was evident between the two components. In the cases reported in Kabra et al. [36] and current case 2, the swellings were multilayered, with no necrotic component within the lesion (Supplementary material 2–14).

At first onset, undifferentiated mesenchymal round cells were positive for CD99 and vimentin, whereas cartilage cells were positive for S100. Ki67 expression levels were 5%, 10%, and 30% in current case 4, case 3, and

another case, respectively [37] (Supplementary material 2–15).

All 36 patients underwent surgery (Supplementary materials 2–16, 17, 18). The prognosis of patients treated with surgery alone and combined adjuvant therapy is shown in the figure and table (Fig. 8e). The prognosis of patients treated with surgery alone and combined adjuvant therapy is significantly different. All patients survived from onset to completion of follow-up, and no metastases were seen elsewhere in the body.

Patients with intraorbital tumors typically present with proptosis. Therefore, we need to differentiate orbital

**Table 1** Ultrasound examination at the time of initial onset

Author	Echo	Distribution	Mixed	Blood flow	Shape	Border	Optic nerve
Cui X et al. 2002	Isoecho	NA	NA	No	NA	Well-defined	NA
Zhang XM et al. 2008	Hypoecho	NA	Punctual hyperecho	NA	NA	NA	NA
Lu P et al. 2017	Hypoecho	Uneven	Presence	NA	NA	Well-defined	NA
Odashiro AN et al. 2007	NA	NA	NA	NA	NA	Well-defined	NA
Current case 2	Isoecho to hypoecho	Uneven	Mass hyperecho	No	Irregular	Unclear	Compression
Current case 3	Hypoecho	Uneven	mass or patchy isoecho or hyperecho	No	Irregular	Well-defined	Compression
Current case 4	Isoecho to hypoecho	Uneven	mass isoecho or hyperecho	NA	Irregular	Well-defined	Compression

NA, Not Available

MC from other tumors. Histopathology and immunohistochemistry are important for differential diagnosis, and the cytogenetic technique of tumors is a significant adjunctive approach (Supplementary material 2–19). Compared with other sites of MC, the prognosis of orbital MC is relatively good. Recurrence indicates the worst outcome. No cases of metastasis or death has been reported.

#### Findings based on MC-related pathways

In this study, 2/5 specimens were positive for *HEY1-NCOA2*, and one specimen was excluded because of decalcification. Although the *HEY1-NCOA2* fusion gene was detected in two other specimens by FISH, the percentage of positive cells was less than 20%. In the study of Wang et al. [8], 7 of 11 specimens were positive. In the 10 FFPE specimens of whole body bones and soft tissues from abdominal wall or extremities reported by Robert et al. [7], eight tested positive. Robert et al. hypothesized that the chromosomes in the samples were damaged at some point in the preparation process, resulting in some of the samples being negative. A larger sample size is needed to clarify the proportion and causes of negatives.

*HEY1-NCOA2* promotes sarcomagenesis by influencing many downstream pathways. The combination of these dysregulated pathways may drive the pathophysiology of MC. Exploring the mechanisms governed by this fusion may help clarify illness etiology and lead to the discovery of new MC treatment targets.

The Notch signaling pathway promotes tumorigenesis through apoptosis, proliferation, and epithelial–mesenchymal transition. Qi et al. [5] used genome-wide chromatin immunoprecipitation sequencing (ChIP-seq) and expression profiling (RNA-seq) to discover that *HEY1*-repressed target genes may be transactivated in the presence of the *HEY1-NCOA2* fusion protein. *HEY1* represses target genes of the Notch pathway. As a member of the Notch pathway, the expression of *COL2A1* is reduced [4]. In our study, *COL2A1* expression was high

in tissues positive for the *HEY1-NCOA2* fusion gene, which validated the above findings.

In the present study, we demonstrated the relatively high expression of  $\beta$ -catenin and APC in *HEY1-NCOA2*-positive tissues. Typical APC gene mutations resulting in abnormalities of the Wnt pathway are less likely to occur in tissues positive for the fusion gene *HEY1-NCOA2* than in tissues negative for the fusion gene.

Wnt signaling is crucial in bone formation and remodeling. It is proposed to affect the mesenchymal precursor cell toward preferential bone formation and inhibition of chondrocyte differentiation. Our immunohistochemical results showed high positivity of cells for  $\beta$ -catenin and APC in the region full of undifferentiated mesenchymal cells. Fanburg-Smith et al. [38] identified the presence of  $\beta$ -catenin in the nucleus at the interface between the undifferentiated mesenchymal round cell region and the cartilage region in MC. This discovery suggested the possibility that the APC/Wnt pathway may be involved in endochondral ossification. APC protein expression was significantly elevated in the fusion gene *HEY1-NCOA2*-positive group. This result suggested that the formation of *HEY1-NCOA2* inhibits cartilage formation by increasing the expression of APC.

PKC- $\alpha$  activation can phosphorylate Bcl-2 and subsequently slow down apoptosis. Bcl2 is highly expressed in MC, especially in undifferentiated mesenchymal cells. In addition, our study found that the *HEY1-NCOA2*-positive group expressed higher Bcl2 than the negative group. Moreover, *HEY1-NCOA2* fusion protein can directly activate Bcl2 in trans [5]. The important role of Bcl2 family members in chemoresistance in conventional chondrosarcoma has been elucidated. Inhibition of Bcl2 family members restores apoptotic mechanisms in MC, sensitizing cells to conventional chemotherapy. Therefore, patients may benefit from a combination of Bcl2 family inhibitors and chemotherapy. By contrast, *HEY1-NCOA2*-positive patients may receive Bcl2 family inhibitors with pronounced effects because of the high expression of Bcl2.

**Table 2** CT and MRI examination at the time of initial onset

CT		MRI														
Density	Soft-tissue	T1-weighted image		T2-weighted image		Isointense		Hypointense		Hyperintense		Distribution		Enhancement		
	NA	Uniform	Uneven, mixed hyperdense	NA	NA	NA	Hypointense	Hypointense	Hyperintense	Hyperintense	Isointense	NA	Uneven, both hypointense on T1 and T2-weighted image	NA	The part other than A is obvious	
9	19	1	19	9	4	7	5	1	4	7	4	4	5	11	9	7

CD99 can activate MAPK pathway mediators through the PKC pathway, thereby regulating cell growth and survival. Aberrant MAPK signaling can promote the development of cancer. Our results showed higher expression of CD99 in *HEY1-NCOA2*-positive patients than in *HEY1-NCOA2*-negative patients. Thus, the MAPK pathway can be activated in the positive patients.

Our research demonstrated that the expression of PAI-1 was higher than that of p-SMAD2. This situation may imply that PAI-1 may also be affected by other signaling pathways, such as the EGFR signaling pathway. Findings of Beaino et al. [4] showed that p-SMAD1 and PAI-1 are highly expressed in about half of the mesenchymal cell component and one-third of the cartilage component.

In summary, the expression of COL2A1 [4] and Bcl2 is elevated in *HEY1-NCOA2*-positive tissues, and they promote tumor cell growth by regulating cell proliferation, apoptosis, epithelial–mesenchymal transition, and drug resistance. We speculate that patients with *HEY1-NCOA2*-positive MC have a poorer prognosis than their counterparts, and combination therapy is necessary for such individuals. For *HEY1-NCOA2*-positive patients, given the high expression of CD99, drugs targeting the MAPK pathway may be an effective treatment. To complement the evidence, differential expressed genes and pathway enrichment analyses were performed using public dataset (GSE163291). Inconsistent results may be due to limited sample types and sizes (Supplementary material 1–2).

Orbital MC is uncommon, and its pathophysiology is poorly understood. In the last 5 years, we have only collected four cases. Given that some of the paraffin-embedded tissues samples had been preserved for a long time, we were unable to validate the fusion gene *HEY1-NCOA2* and pathway-related markers at the RNA level. We evaluated these cases in conjunction with those reported by other experts to gain a thorough understanding of MC. Additional fresh tissues must be collected for an in-depth investigation of MC and its specific *HEY1-NCOA2* fusion gene-related pathways.

### Conclusions

We summarized the clinical features, treatments, and prognosis of MC occurring in orbital soft tissue, including our cases and the literature. Orbital MC is characterised by proptosis, loss of vision, and optic papilla oedema, often occurring in the superior medial and superior lateral quadrants. Patients with *HEY1-NCOA2*-positive MC have a poorer prognosis than those without it, and for such patients, combination therapy is necessary. Drugs targeting the MAPK pathway might be an effective treatment.

## Abbreviations

MC	Mesenchymal chondrosarcoma
RCA-FISH	Rolling circle amplification fluorescence in situ hybridization
HE	Hematoxylin–eosin
Notch1	Notch homolog 1
COL2A1	Collagen Type II
WNT3A	Wingless/Integrated 3a
PKC- $\alpha$	Protein kinase C
Bcl2	B-cell lymphoma-2
TGF- $\beta$ 1	Transforming growth factor- $\beta$
PAI-1	Plasminogen activator inhibitor-1
p-Smad2	Phospho-Smad2
p-Smad1	Phospho-Smad1
AKT	Protein kinase B
PI3K	Phosphoinositide 3-kinase
HES1	Hairy and enhancer of split 1
T1WI	T1-weighted image
T2WI	T2-weighted image

## Supplementary Information

The online version contains supplementary material available at <https://doi.org/10.1186/s12886-025-04082-z>.

Supplementary Material 1

Supplementary Material 2

## Acknowledgements

Not applicable.

## Author contributions

LJQ and LX contributed equally to this work and should be regarded as co-first authors. LJQ and LX collected data, completed the experiments, and wrote the main manuscript text. ZJZ critically reviewed the study proposal. WQ analyzed and identified the accuracy of the results and discussions presented in the manuscript. ZLM and LTT contributed equally to this work and should be regarded as co-corresponding authors. ZLM and LTT designed the study and was responsible for review and revision of the manuscript. All authors read and approved the final manuscript.

## Funding

This work was supported by the Open Project of Tianjin Key Laboratory of Retinal Functions and Diseases (2021tjswmm001), Tianjin Health Science and Technology Project (TJWJ2022MS012) and Tianjin Key Medical Discipline (Specialty) Construction Project (TJYXZDXK-037 A).

## Data availability

The datasets used and/or analyzed during the current study are available from the corresponding author on reasonable request.

## Declarations

### Ethical approval

This study was approved by Medical Ethics Committee of Tianjin Medical University Eye Hospital (2022KY [L]-59) All adult study participants or their guardians voluntarily signed an informed consent form.

### Consent for publication

Not applicable.

### Competing interests

The authors declare no competing interests.

Received: 4 April 2024 / Accepted: 16 April 2025

Published online: 29 April 2025

## References

- Lichtenstein L, Lichtenstein L, Bernstein D. Unusual benign and malignant chondroid tumors of bone. A survey of some mesenchymal cartilage tumors and malignant chondroblastic tumors, including a few multicentric ones, as well as many atypical benign chondroblastomas and chondromyxoid fibromas. *Cancer*. 1959. [https://doi.org/10.1002/1097-0142\(195911/12\)12:6%3C1142::aid-cnrcr2820120610%3E3.0.co;2-d](https://doi.org/10.1002/1097-0142(195911/12)12:6%3C1142::aid-cnrcr2820120610%3E3.0.co;2-d).
- Reeh MJ. Hemangiopericytoma with cartilaginous differentiation involving orbit. *Arch Ophthalmol*. 1966. <https://doi.org/10.1001/archoph.1966.00970050084016>.
- Alam MS, Subramanian N, Desai AS, Krishnakumar S. Mesenchymal chondrosarcoma of the orbit: A case report with 5 years of follow-up. *Orbit*. 2018;37:73–5. <https://doi.org/10.1080/01676830.2017.1353116>.
- El Beaino M, Roszik J, Livingston JA, et al. Mesenchymal chondrosarcoma: a review with emphasis on its Fusion-Driven biology. *Curr Oncol Rep*. 2018;20:37. <https://doi.org/10.1007/s11912-018-0668-z>.
- Qi W, Rosikiewicz W, Yin Z, et al. Genomic profiling identifies genes and pathways dysregulated by HEY1–NCOA2 fusion and shines a light on mesenchymal chondrosarcoma tumorigenesis. *J Pathol*. 2022;257:579–92. <https://doi.org/10.1002/path.5899>.
- Larsson C, Koch J, Nygren A, Janssen G, Raap AK, Landegren U, Nilsson M. In situ genotyping individual DNA molecules by target-primed rolling-circle amplification of padlock probes. *Nat Methods*. 2004;1:227–32. <https://doi.org/10.1038/nmeth723>.
- Nakayama R, Miura Y, Ogino J, Susa M, et al. Detection of HEY1–NCOA2 fusion by fluorescence in-situ hybridization in formalin-fixed paraffin-embedded tissues as a possible diagnostic tool for mesenchymal chondrosarcoma: HEY1–NCOA2 in mesenchymal chondrosarcoma. *Pathol Int*. 2012;62:823–6. <https://doi.org/10.1111/pin.12022>.
- Wang L, Motoi T, Khanin R, et al. Identification of a novel, recurrent HEY1–NCOA2 fusion in mesenchymal chondrosarcoma based on a genome-wide screen of exon-level expression data. *Genes Chromosom Cancer*. 2012;51:127–39. <https://doi.org/10.1002/gcc.20937>.
- Herrera A, Ortega C, Reyes G, Alvarez MA, Tellez D. Primary orbital mesenchymal chondrosarcoma: case report and review of the literature. *Case Rep Med*. 2012;2012:1–4. <https://doi.org/10.1155/2012/292147>.
- Odashiro AN, Leite LVO, Oliveira RS, et al. Primary orbital mesenchymal chondrosarcoma: a case report and literature review. *Int Ophthalmol*. 2009;29:173–7. <https://doi.org/10.1007/s10792-007-9184-0>.
- Lu P, Xiao W, Gao Y, Mao Y. Primary orbital mesenchymal chondrosarcoma. *Can J Ophthalmol*. 2018;53:e205–7. <https://doi.org/10.1016/j.jco.2017.11.008>.
- Alkatan HM, Eberhart CG, Alshomar KM, Elkhamary SM, Maktabi AMY. Primary mesenchymal chondrosarcoma of the orbit: histopathological report of 3 pediatric cases. *Saudi J Ophthalmol*. 2018;32:69–74. <https://doi.org/10.1016/j.sjopt.2018.02.016>.
- D'Ali L, Tulliso A, Mariuzzi L. Primary mesenchymal chondrosarcoma of the orbit in a young female: imaging and histopathological features. *J Surg Case Rep*. 2020;2020:rjaa037. <https://doi.org/10.1093/jscr/rjaa037>.
- Yap E, Cabrera S, Bojador M, Sy Ortin T, Bacorro W. Orbital mold brachytherapy for recurrent orbital mesenchymal chondrosarcoma: a case report. *Jcb*. 2021;13:694–700. <https://doi.org/10.5114/jcb.2021.112121>.
- Kabra R, Patel S, Shanbhag S. Orbital chondroma: A rare mesenchymal tumor of orbit. *Indian J Ophthalmol*. 2015;63:551. <https://doi.org/10.4103/0301-4738.162638>.
- Razak ARA, Gurney L, Kirkham N, Lee D, Neoh C, Verrill M. Mesenchymal chondrosarcoma of the orbit: an unusual site for a rare tumour: mesenchymal chondrosarcoma of the orbit. *Eur J Cancer Care*. 2009;19:551–3. <https://doi.org/10.1111/j.1365-2354.2008.01028.x>.
- Font RL, Ray R, Mazow ML, Del Valle M. Mesenchymal chondrosarcoma of the orbit: A unique Radiologic-Pathologic correlation. *Ophthal Plast Reconstr Surg*. 2009;25:219–22. <https://doi.org/10.1097/OP.0b013e3181a142fc>.
- Gobert D, Patey N, Doyon J, Kalin-Hajdu E. Mesenchymal chondrosarcoma of the orbit masquerading as a hemophilic pseudotumor. *Orbit*. 2021;40:431–4. <https://doi.org/10.1080/01676830.2020.1812093>.
- Bagheri A, Abbaszadeh M, Torbati P, Rezaei Kanavi M. Mesenchymal chondrosarcoma of the orbit attached to the optic nerve. *J Craniofac Surg*. 2018;29:e591–4. <https://doi.org/10.1097/SCS.0000000000004635>.
- Lü H-B, Yang Y-L, Luo Q-L, He W-M. Mesenchymal chondrosarcoma of the orbit: report of a case and review of the literature. 2008.
- Patel R, Mukherjee B. Mesenchymal chondrosarcoma of the orbit. *Orbit*. 2012;31:126–8. <https://doi.org/10.3109/01676830.2011.638097>.

22. Hanakita S, Kawai K, Shibahara J, Kawahara N, Saito N. Mesenchymal chondrosarcoma of the orbit. *Neurol Med Chir*. 2012. <https://doi.org/10.2176/nmc.52.747>.
23. Angotti-Neto H, Cunha LP, Oliveira ÂV, Monteiro MLR. Mesenchymal chondrosarcoma of the orbit. *Ophthal Plast Reconstr Surg*. 2006;22:378–82. <https://doi.org/10.1097/01.iop.0000229691.87499.99>.
24. Kiratli H, Deniz Y, Büyükerem B, Gedikoğlu G. Mesenchymal chondrosarcoma of the lacrimal gland. *Ophthalmic Plast Reconstr Surg*. 2018 May/ Jun;34(3):e77–9. <https://doi.org/10.1097/IOP.0000000000001054>
25. Jakhetiya A, Shukla NK, Muduly D, Kale SS. Extraskelatal orbital mesenchymal chondrosarcoma: surgical approach and mini review. *Bmj Case Rep*. 2017;bcr2016218744. <https://doi.org/10.1136/bcr-2016-218744>.
26. Szumera-Ciećkiewicz A, Ptasiński K, Grabowski P, Krajewski R, Tacikowska M. Correct answer to the quiz. Check your diagnosis. [In.d.].
27. Tuncer S, Kebudi R, Peksayar G, et al. Congenital mesenchymal chondrosarcoma of the orbit. *Ophthalmology*. 2004;111:1016–22. <https://doi.org/10.1016/j.ophtha.2003.12.026>.
28. Liu M, Qin W, Yin Z. An unusual case of primary mesenchymal chondrosarcoma in orbit with intracranial extension. *Clin Imag*. 2010;34:379–81. <https://doi.org/10.1016/j.clinimag.2009.12.002>.
29. Bonavolonta P, Strianese D, Maria Luisa Vecchione MM, Staibano S. A challenging case of primary orbital mesenchymal chondrosarcoma. *Orbit*. 2010;29:281–3. <https://doi.org/10.3109/01676831003664327>.
30. Zhang X-M, Duan J-G, Cao S-Q, Zheng F-L. A case of intraorbital mesenchymal chondrosarcoma. *Journal Clin Ophthalmology*. 2008;16:242–1. <https://doi.org/10.3969/j.issn.1006-8422.2008.03.036>.
31. Zhou H, Xue L-M. Report of a case of orbital mesenchymal chondrosarcoma. *J Kunming Med Univ*. 2009;30:149–2. <https://doi.org/10.3969/j.issn.1003-4706.2009.10.045>.
32. Cui X, Wang W-G, Liu S-Z. A case of chondrosarcoma of the soft tissue mesenchyme of the orbit. *Chin J Practical Ophthalmol*. 2002;20:959–2. <https://doi.org/10.3760/cmaj.issn.1006-4443.2002.12.054>.
33. Naama O, Aija A, El Moustarchid B, et al. Chondrosarcome mésochymateux sphéno-orbitaire. A Propos D'un Cas [Spheno-orbital mesenchymal chondrosarcoma. A Case report]. *J Fr Ophtalmol*. 2007;30(2):211–5. [https://doi.org/10.1016/s0181-5512\(07\)89579-9](https://doi.org/10.1016/s0181-5512(07)89579-9). French.
34. Wang T-G, Qin W, Xie H-P. A case of orbital mesenchymal chondrosarcoma. *J Army Med Univ*. 2006;28:2083–1.
35. Liu H-X, Gao P, Liang L, Xing D-H, Zhang Y-K. A case of orbital mesenchymal chondrosarcoma. *Recent Adv Ophthalmol*. 2008;228:303–1.
36. Kaur A, Kishore P, Agrawal A, Gupta A. Mesenchymal chondrosarcoma of the orbit: A report of two cases and review of the literature. *Orbit*. 2008;27:63–7. <https://doi.org/10.1080/01676830601169007>.
37. Hanakita S, Kawai K, Shibahara J, Kawahara N, Saito N. Mesenchymal chondrosarcoma of the orbit. *Neurol Med Chir*. 2012;4. <https://doi.org/10.2176/nmc.52.747>.
38. Fanburg-Smith JC, Auerbach A, Marwaha JS, Wang Z, Rushing EJ. Reappraisal of mesenchymal chondrosarcoma: novel morphologic observations of the hyaline cartilage and endochondral ossification and  $\beta$ -catenin, Sox9, and osteocalcin immunostaining of 22 cases. *Hum Pathol*. 2010;41:653–62. <https://doi.org/10.1016/j.humpath.2009.11.006>.

### Publisher's note

Springer Nature remains neutral with regard to jurisdictional claims in published maps and institutional affiliations.